Quartic Anharmonicity of Rattlers and Its Effect on Lattice Thermal Conductivity of Clathrates from First Principles

Terumasa Tadano[1,2,*] and Shinji Tsuneyuki[3,4]
[1]International Center for Young Scientists (ICYS), National Institute for Materials Science, Tsukuba 305-0047, Japan
[2]Research and Services Division of Materials Data and Integrated System (MaDIS), National Institute for Materials Science, Tsukuba 305-0047, Japan
[3]Department of Physics, The University of Tokyo, Tokyo 113-0033, Japan
[4]Institute for Solid State Physics, The University of Tokyo, Kashiwa 277-8581, Japan

(Received 4 October 2017; revised manuscript received 10 December 2017; published 7 March 2018)

We investigate the role of the quartic anharmonicity in the lattice dynamics and thermal transport of the type-I clathrate $Ba_8Ga_{16}Ge_{30}$ based on *ab initio* self-consistent phonon calculations. We show that the strong quartic anharmonicity of rattling guest atoms causes the hardening of vibrational frequencies of low-lying optical modes and thereby affects calculated lattice thermal conductivities κ_L significantly, resulting in an improved agreement with experimental results including the deviation from $\kappa_L \propto T^{-1}$ at high temperature. Moreover, our static simulations with various different cell volumes shows a transition from crystal-like to glasslike κ_L around 20 K. Our analyses suggest that the resonance dip of κ_L observed in clathrates with large guest free spaces is attributed mainly to the strong three-phonon scattering of acoustic modes along with the presence of higher-frequency dispersive optical modes.

DOI: 10.1103/PhysRevLett.120.105901

Intermetallic clathrates are a class of materials possessing a cagelike structure incorporating a guest atom, which is loosely bound inside an oversized cage and makes a large amplitude thermal vibration called "rattling." Experimental and theoretical studies have evidenced that rattling guest atoms cause the characteristic lattice dynamics of clathrates including the low-frequency vibrational modes showing a significant temperature T dependence [1–4] and very low lattice thermal conductivity (LTC) κ_L [3,5,6]. LTCs of clathrates are not only very low but also show an exceptional and diverse T dependence. For example, κ_L of the electron-doped type-I clathrate $Ba_8Ga_{16}Ge_{30}$ (BGG) shows a peak around 20 K followed by a decreasing region at higher temperature [7,8], just like many crystalline solids. However, in the temperature region above ~100 K, the T dependence is much milder than $\kappa_L \propto T^{-1}$ of typical crystalline materials [9]. A more exceptional T dependence has been reported for the type-I clathrates $X_8Ga_{16}Ge_{30}$ ($X = $ Sr, Eu) [7,10] and $Ba_8Ga_{16}Sn_{30}$ [11]. In these materials, the LTCs behave like a typical glass, showing a plateau region or a "resonance dip" [10] near ~20 K, an increasing trend in ~20–100 K, and a nearly T-independent region above 100 K. This unconventional and diverse thermal transport in intermetallic clathrates has been attributed to the difference in the guest free space of the rattling atoms [7,12,13], the host-guest coupling strength [14,15], and the magnitude of static or dynamical disorders [14,16]. Despite these continuous efforts, the origin of the unusual LTCs of clathrates still remains unclear.

Recently, an *ab initio* calculation of the LTC based on the Peierls-Boltzmann theory [17] has established itself as a convenient way to predict or analyze thermal transport phenomena in solids [18]. Although the validity of the Boltzmann theory is limited to the cases where the phonon quasiparticle picture is well established [19], it has reproduced the experimental LTC of BGG in a relatively low temperature region [6]. However, the *ab initio* Boltzmann approach considerably underestimated κ_L above ~100 K. A similar underestimation has also been reported in a more recent study on another type-I clathrate, $Ba_{7.81}Ge_{40.67}Au_{5.33}$ [20]. These results clearly indicate the necessity of an improved theoretical approach. One of the most problematic approximations made in the conventional Boltzmann approach is the omission of the quartic anharmonicity. Indeed, the atomic displacement factor of guest atoms is so significant that the quartic anharmonicity cannot be neglected anymore in a clathrate.

Here, we report the volume and temperature dependence of κ_L of the type-I clathrate BGG obtained from a first-principles calculation, where the temperature renormalization of the vibrational frequency by the quartic anharmonicity is considered using the self-consistent phonon (SCP) theory [21–26]. We show that the strong quartic anharmonicity of rattling motions makes the deviation from

$\kappa_L \propto T^{-1}$ at high temperature. Our computational analyses also indicate that the resonance dip observed in clathrates with large cage sizes can be attributed to the strong three-phonon scattering of acoustic modes along with the presence of high-frequency dispersive optical modes and the phonon-boundary scatterings.

We start by giving a brief overview of the SCP method. Following our recent implementation [25], we calculate the T-dependent anharmonic frequencies $\Omega_q(T)$ and polarization vectors $\boldsymbol{\epsilon}_q(T)$ by diagonalizing the matrix $\boldsymbol{V_q}$ defined as

$$V_{\boldsymbol{q}jj'} = \omega^2_{\boldsymbol{q}j}\delta_{jj'} + \frac{1}{2}\sum_{q_1}\Phi(\boldsymbol{q}j;-\boldsymbol{q}j';q_1;-q_1)\langle Q^*_{q_1}Q_{q_1}\rangle. \quad (1)$$

Here, $\omega_{\boldsymbol{q}j}$ is the harmonic phonon frequency with the crystal momentum $\boldsymbol{q}$ and the branch index j, and q is the shorthand notation for $(\boldsymbol{q}, j)$ satisfying $q = (\boldsymbol{q}, j)$ and $-q = (-\boldsymbol{q}, j)$. $\Phi(\boldsymbol{q}j;-\boldsymbol{q}j';q_1;-q_1)$ is the reciprocal representation of the fourth-order interatomic force constants (IFCs). $\langle Q^*_q Q_q\rangle = [\hbar/(2\Omega_q)][1 + 2n(\Omega_q)]$ is the mean square displacement of the normal coordinate Q_q, where $n(\omega) = 1/(e^{\beta\hbar\omega} - 1)$ is the Bose-Einstein distribution function, $\beta = 1/kT$ with the Boltzmann constant k, and $\hbar$ is the reduced Planck constant. The frequency renormalization by the SCP theory includes the effect of an infinite set of Feynman diagrams generated from the loop diagram, which is a first-order correction by the quartic anharmonicity [27]. Therefore, it should be more important than the four-phonon scattering, which is a second-order correction, especially for low-κ_L materials. More details about the present SCP formalism are described elsewhere [25,27].

All of the density-functional theory (DFT) calculations were conducted using the VASP code [28], with the Perdew-Burke-Ernzerhof functional [29] and the projector augmented wave method [30,31], and the phonon calculations were performed using the ALAMODE package [32,33]. An ordered unit cell containing 54 atoms (space group $Pm\bar{3}n$) was employed for modeling lattice anharmonicity and phonon thermal transport. To investigate the effect of the guest free space on phonon properties, the lattice constant of BGG was compressed or expanded from the optimized value (10.954 Å, hereafter called "opt.") by −2% to +6% in steps of 2%. Harmonic and anharmonic IFCs were estimated using the compressive sensing lattice dynamics method [34]. More detailed computational procedures are provided in the Supplemental Material [35].

Calculated harmonic phonon dispersion curves of BGG in the low-frequency region ($\lesssim 80$ cm^{-1}) are shown in Fig. 1(a) by dotted lines. With increasing lattice constant,

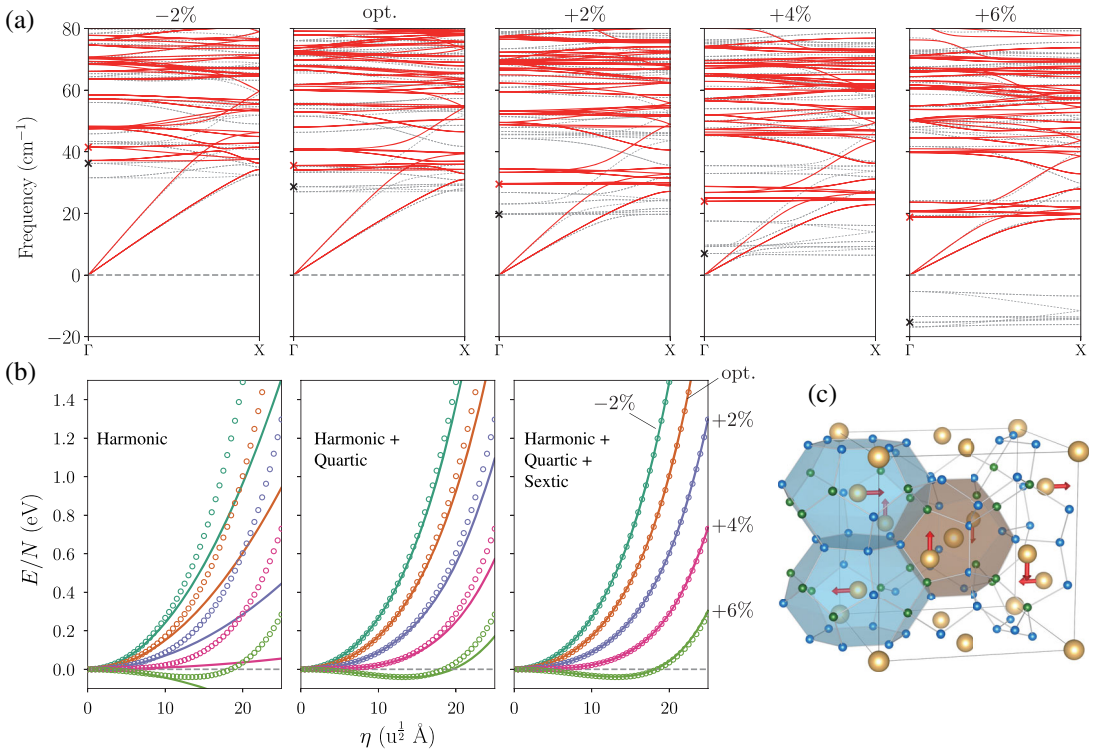

FIG. 1. Lattice dynamics of the type-I clathrate $Ba_8Ga_{16}Ge_{30}$ with various lattice constants. (a) Phonon dispersion curves in the low-frequency region along the Γ-X line. The dotted lines show the harmonic phonon frequencies and the solid lines are the result of the SCP calculations at 300 K. The cross symbols "times" indicate the positions of the lowest Raman active T_{2g} modes. (b) Potential energy surface of the lowest T_{2g} mode. The circles "open circle" represent the results of DFT calculations and the lines are obtained from the harmonic and anharmonic force constants. (c) Crystal structure of $Ba_8Ga_{16}Ge_{30}$ (with VESTA [42]). The red arrows indicate the displacement pattern of the T_{2g} mode.

the frequencies of the low-lying optical modes associated with rattlers decrease. In the largest-volume case, twelve phonon modes become unstable ($\omega_q^2 < 0$), all of which can be well characterized as collective motions of Ba(2) atoms inside the tetrakaidecahedral cages [see Fig. 1(c)]. To see the volume dependence of the lattice anharmonicity more directly, we also calculated the potential energy surface (PES) of the Raman active T_{2g} guest mode by displacing atoms by $\boldsymbol{u}_\kappa = M_\kappa^{-1/2}\boldsymbol{e}_{q,\kappa}\eta$ with η being the amplitude of the normal coordinate of the T_{2g} mode. In Fig. 1(b), we compare the PESs calculated by DFT and those calculated from the IFCs. The left panel of Fig. 1(b) shows that the harmonic approximation fails to capture the actual shape of the PES, indicating the significance of the anharmonicity. Indeed, if we include the contribution from the fourth-order IFCs, we obtain overall good agreements with the DFT results [middle panel of Fig. 1(b)]. Moreover, the sixth-order IFCs further improve the accuracy of the Taylor expansion potential [right panel of Fig. 1(b)]. Since the correction by the sextic terms is minor, however, we only considered the dominant quartic terms in the SCP calculations.

We calculated finite-temperature phonon dispersion curves by solving the SCP equation [Eq. (1)] at various temperatures. The SCP dispersion curves at 300 K are shown in Fig. 1(a) by solid lines. The quartic anharmonicity generally increases the frequencies of the low-lying rattling modes, which can be attributed to the dominant and positive contribution from the diagonal term of the quartic coefficient; $\Phi(\mathbf{0}j;\mathbf{0}j;\mathbf{0}j;\mathbf{0}j) > 0$ for the low-lying optical modes j. With increasing cage size, the quartic component of the PES becomes more important as shown in Fig. 1(b), leading to the greater frequency shifts. For the higher-frequency modes above 80 cm^{-1}, the anharmonic renormalization turned out to be relatively small (see the Supplemental Material [35]). The present result is the first realization of the *ab initio* SCP calculation for a complex host-guest structure.

According to the Raman study of Takasu *et al.* [1], the frequency of the T_{2g} guest mode in BGG increases from 31 cm^{-1} at 2 K to 34 cm^{-1} at room temperature. The SCP theory for the opt case gives 29.8 cm^{-1} at 0 K and 35.5 cm^{-1} at 300 K, which agree well with the experimental values especially given that the present SCP theory neglects the intrinsic frequency shift by the cubic anharmonicity and the quasiharmonic effect. To investigate the significance of the intrinsic frequency shift by the cubic terms, we also calculated the lowest-order correction by the cubic anharmonicity from the real part of the bubble self-energy as $\Delta_q = -\mathrm{Re}\Sigma_q^{(B)}(\Omega_q)$ with $\Sigma_q^{(B)}(\omega)$ defined as

$$\Sigma_q^{(B)}(\omega) = \frac{\hbar}{2N}\sum_{q_1,q_2,s=\pm1}{}' \frac{|\Phi(-q;q_1;q_2)|^2}{8\Omega_q\Omega_{q_1}\Omega_{q_2}} \times\left(\frac{n_1+n_2+1}{s\omega_c+\Omega_{q_1}+\Omega_{q_2}} - \frac{n_1-n_2}{s\omega_c+\Omega_{q_1}-\Omega_{q_2}}\right). \quad (2)$$

Here, N is the number of $\boldsymbol{q}$ points in the first Brillouin zone, $n_i = n(\Omega_{q_i})$, $\omega_c = \omega + i0^+$ with 0^+ being a positive infinitesimal, and the summation over (q_1, q_2) is restricted to the pairs satisfying the momentum conservation; $\boldsymbol{q} \pm \boldsymbol{q}_1 = \boldsymbol{q}_2 + \boldsymbol{G}$. For the opt case, the Δ_q value of the T_{2g} mode calculated with the $9\times9\times9\boldsymbol{q}$ point mesh was -0.2 cm^{-1} at 0 K and -1.1 cm^{-1} at 300 K. Hence, the experimental T dependence of the Raman shift can be better explained with the inclusion of the effect of the intrinsic frequency shift by the cubic anharmonicity. We have also calculated the Δ_q values for the other systems with different cage sizes and have found that the frequency shift by the bubble diagram is negative ($\Delta_q < 0$) and less significant than the hardening by the quartic anharmonicity [35].

To elucidate the intrinsic effects of the frequency renormalization on the LTC quantitatively, we have calculated κ_L based on the Boltzmann transport equation (BTE) within the relaxation-time approximation, where

$$\kappa_L^{\mu\nu}(T) = \frac{1}{NV}\sum_q c_q(T)v_q^\mu(T)v_q^\nu(T)\tau_q(T). \quad (3)$$

Here, V is the unit cell volume, $c_q(T)$ is the mode specific heat, $\boldsymbol{v}_q(T)$ is the group velocity, and $\tau_q(T)$ is the lifetime of phonon q. Unlike the conventional BTE approach, where harmonic frequencies and eigenvectors are used as the ground state for calculating $\boldsymbol{v}_q$ and τ_q, we employ the SCP frequencies and eigenvectors in the present SCP + BTE method [Eq. (3)]. Therefore, the group velocity $\boldsymbol{v}_q(T) = \partial\Omega_q(T)/\partial\boldsymbol{q}$ also shows an intrinsic T dependence. The phonon lifetime τ_q is estimated using Matthiessen's rule $\tau_q^{-1} = \tau_{q,\mathrm{anh}}^{-1} + \tau_{q,\mathrm{iso}}^{-1} + \tau_{q,b}^{-1}$. The anharmonic scattering rate is calculated from the imaginary part of the bubble self-energy [Eq. (2)] as $\tau_{q,\mathrm{anh}}^{-1} = 2\Gamma_q^{(B)} = 2\mathrm{Im}\Sigma_q^{(B)}(\Omega_q)$, and the phonon-isotope scattering rate $\tau_{q,\mathrm{iso}}^{-1}$ is evaluated perturbatively [43]. For the phonon-boundary scattering rate, we employ $\tau_{q,b}^{-1} = 2|\boldsymbol{v}_q|/L$ with the grain size of $L = 2.5$ μm that reproduces the experimental crystalline peak of the LTC [7].

Figure 2 shows the (V,T) dependence of the LTC calculated by the BTE and the SCP + BTE methods with $9\times9\times9\boldsymbol{q}$ points. The LTC values calculated by the SCP + BTE method are generally higher than those obtained by the conventional BTE method. This tendency becomes more pronounced with increasing V and T. The predicted κ_L value by the SCP + BTE method is 0.97 W/mK at 300 K, which agrees well with the experimental values of 1.31 W/mK (Sales *et al.*, Ref. [7]) and 1.06 W/mK (May *et al.*, Ref. [9]). In contrast, the conventional method gives 0.58 W/mK, which is 40% smaller than the SCP + BTE value. Moreover, the deviation from $\kappa_L \propto T^{-1}$ in a high temperature range can be well reproduced by the

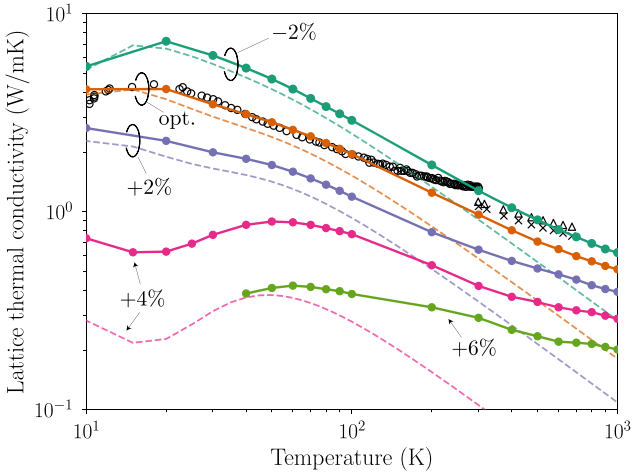

FIG. 2. Lattice thermal conductivity of BGG calculated with various lattice constants. The solid and dashed lines are obtained with the SCP + BTE method and the conventional BTE method, respectively. The experimental values in the low- (open circle) and high-temperature (times, triangle) regions are adapted from Refs. [7,9], respectively.

SCP + BTE approach. These results clearly reveal the essential role of the frequency renormalization on the thermal transport properties of BGG. To elucidate the origin of the increase in κ_L due to the hardening of the guest modes, we compare the LTC spectrum $\kappa_L(\omega)$ for the opt case at 300 K. The results are shown in Fig. 3(a). With the hardening of the low-lying guest modes, $\kappa_L(\omega)$ increases significantly in the frequency region below 70 cm^{-1}. After careful investigation, we found that this increase can be ascribed to the decrease in the phonon linewidth $\Gamma_q^{(B)}$, whose magnitude is roughly proportional to the available scattering phase space (SPS) and the strength of the cubic coupling $|V^{(3)}(-q;q_1;q_2)|^2 = |\Phi(-q;q_1;q_2)|^2/8\Omega_q\Omega_1\Omega_2$. In the frequency range of 45–65 cm^{-1}, the SPS decreases by ~50% due to the hardening of the low-frequency guest modes [35]. This reduction results in the enhancement of $\kappa_L(\omega)$ in the same frequency range. In the low-frequency region below 45 cm^{-1}, however, the change of the SPS is too small to explain the corresponding enhancement of $\kappa_L(\omega)$. Indeed, we found that the coupling coefficient $|V^{(3)}(-q;q_1;q_2)|^2$ is also suppressed strongly due to the reduction of the optical-acoustic phonon hybridization caused by the hardenings of the optical modes (see the Supplemental Material [35]). The reduction of $\Gamma_q^{(B)}$ by the anharmonic renormalization observed here highlights the importance of the (effective) harmonic force constants, in accord with the previous numerical and experimental studies [44–46]. We have also found that, with the inclusion of the effect of the frequency renormalization, the theoretical $\Gamma_q^{(B)}$ values of the TA modes agree quantitatively with the experimental results of Lory *et al.* [20] at 300 K (see the Supplemental Material [35]).

Next, we discuss the volume dependence of the LTC calculated by the SCP + BTE method. As can be inferred from Fig. 2, the LTC values decrease with increasing unit cell volume. It is interesting to observe that the crystalline peak of κ_L near 20 K evolved into a resonance dip when the lattice constant was expanded up to +4%. In the "+4%" system, κ_L takes the minimum value at ~15 K and increases up to 50 K, which is qualitatively different from the T dependence of the other systems. These computational results agree qualitatively with the experimental results on $Sr_8Ga_{16}Si_{30-x}Ge_x$, where the cage size was controlled by changing the x value [12]. To understand the microscopic origin of the increase of κ_L from ~15 to 50 K, we compare the calculated LTC spectra of the "+2%" and +4% systems in Figs. 3(b) and 3(c), respectively. In both systems, the dispersive phonon modes below 50 cm^{-1} contribute more than 90% to the total κ_L value at 20 K. When higher frequency phonon modes are thermally excited at 50 K via the enhancement of $c_q(T)$, the contribution from the dispersive optical modes around 100 cm^{-1} becomes significant. In the +2% system, the thermal enhancement of $\kappa_L(\omega)$ near 100 cm^{-1} was smaller than the concurrent reduction in $\omega < 50$ cm^{-1}, which resulted in $\kappa_L(20\ \mathrm{K}) > \kappa_L(50\ \mathrm{K})$. When the lattice constant is changed from +2% to +4%, the frequencies of the low-lying guest modes decrease as discussed earlier. This softening causes suppression of $\kappa_L(\omega)$, which is particularly significant in $\omega < 50$ cm^{-1} while the phonon lifetimes as well as $\kappa_L(\omega)$ in the higher frequency region (~100 cm^{-1}) are less affected [35]. Such a joint effect of strong acoustic-optical scatterings in the low-frequency

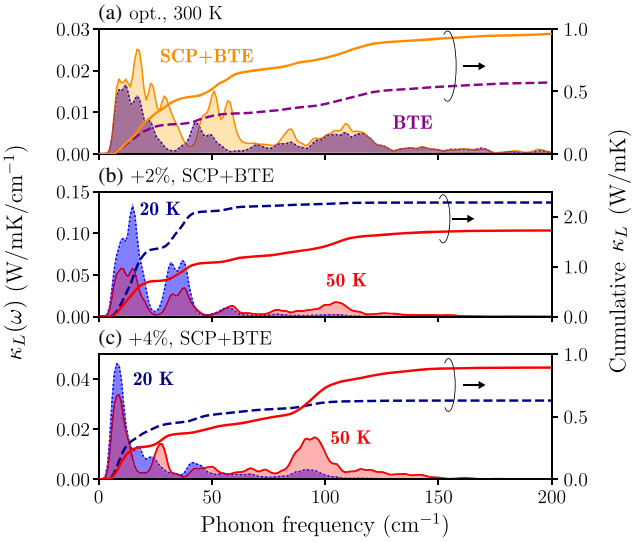

FIG. 3. Thermal conductivity spectrum $\kappa_L(\omega)$ and its cumulative value. (a) Comparison of the conventional BTE and SCP + BTE results for the optimized lattice constant at 300 K. (b),(c) SCP + BTE results for the +2% and +4% systems compared at two different temperatures.

range and the presence of higher-frequency dispersive optical modes resulted in $\kappa_L(20\ \mathrm{K}) < \kappa_L(50\ \mathrm{K})$ for the +4% system. It is important to mention that the predicted κ_L values in the low-T region depend on the employed grain size L. We found that the resonance dip of the +4% system persisted even when we omitted the boundary scattering term. Moreover, the resonance dip changed into a plateau when we employed a smaller L value, which is consistent with the experimental fact that the presence of the resonance dip is sensitive to the details of the sample preparation methods [7,10,16].

Finally, we focus on the T dependence of κ_L above 50 K in Fig. 2. The T dependence obtained by the conventional BTE method follows $\kappa_L \propto T^{-1}$ for all of the studied systems, which do not agree with the experimental fact that κ_L shows weaker T dependence [9,12]. The SCP + BTE method considerably improved the agreement with the experimental results and produced a milder temperature dependence. However, it was still inadequate to reproduce the increasing trend of κ_L observed in some clathrates having large guest free spaces. Since the SCP + BTE method is still based on the phonon-gas model, it does not include the nondiagonal Peierls contribution [19,47] and the anharmonic contribution [48] to the heat flux operator, which become generally more important at high temperature. Therefore, our results also indicate that these contributions may not be negligible in some clathrates at high temperature.

To summarize, we performed fully *ab initio* calculations of κ_L of the type-I clathrate BGG with various different cage sizes, where both the three-phonon scattering and the frequency renormalization by the quartic anharmonicity were taken into account. We showed that the hardening of the vibrational frequencies of rattling modes caused by the quartic anharmonicity significantly affects the calculated κ_L values, leading to an improved agreement with experimental results including the T dependence weaker than $\kappa_L \propto T^{-1}$. In addition, we found that the evolution from crystal-like to glasslike κ_L near ~20 K can be realized by our static calculations without disorders, which can be attributed to the presence of low-frequency guest modes that strongly couple with acoustic modes along with higher-frequency dispersive optical modes and the phonon-boundary scatterings. While our simulation does not exclude the possibility of disorders to further reinforce the glasslike behavior observed in real clathrate samples, it provides a new miscroscopic insight into the exceptional thermal transport of clathrates.

We thank Koichiro Suekuni and Stéphane Pailhès for fruitful discussions, and Kiyoyuki Terakura for useful comments. This study is partly supported by JSPS KAKENHI Grant No. 16K17724, the "Materials research by Information Integration" Initiative (MI2I) project of the Support Program for Starting Up Innovation Hub from Japan Science and Technology Agency (JST), and the MEXT Element Strategy Initiative to Form Core Research Center in Japan. The computation in this work has been done using the facilities of the Supercomputer Center, Institute for Solid State Physics, The University of Tokyo.

*tadano.Terumasa@nims.go.jp

[1] Y. Takasu, T. Hasegawa, N. Ogita, M. Udagawa, M. A. Avila, K. Suekuni, I. Ishii, T. Suzuki, and T. Takabatake, Phys. Rev. B **74**, 174303 (2006).
[2] M. Christensen, A. B. Abrahamsen, N. B. Christensen, F. Juranyi, N. H. Andersen, K. Lefmann, J. Andreasson, C. R. H. Bahl, and B. B. Iversen, Nat. Mater. **7**, 811 (2008).
[3] T. Takabatake, K. Suekuni, T. Nakayama, and E. Kaneshita, Rev. Mod. Phys. **86**, 669 (2014).
[4] J. Wu, K. Akagi, J. Xu, H. Shimotani, K. K. Huynh, and K. Tanigaki, Phys. Rev. B **93**, 094303 (2016).
[5] J. Dong, O. F. Sankey, and C. W. Myles, Phys. Rev. Lett. **86**, 2361 (2001).
[6] T. Tadano, Y. Gohda, and S. Tsuneyuki, Phys. Rev. Lett. **114**, 095501 (2015).
[7] B. C. Sales, B. C. Chakoumakos, R. Jin, J. R. Thompson, and D. Mandrus, Phys. Rev. B **63**, 245113 (2001).
[8] M. A. Avila, K. Suekuni, K. Umeo, H. Fukuoka, S. Yamanaka, and T. Takabatake, Phys. Rev. B **74**, 125109 (2006).
[9] A. F. May, E. S. Toberer, A. Saramat, and G. J. Snyder, Phys. Rev. B **80**, 125205 (2009).
[10] G. S. Nolas, J. L. Cohn, G. A. Slack, and S. B. Schujman, Appl. Phys. Lett. **73**, 178 (1998).
[11] M. A. Avila, K. Suekuni, K. Umeo, H. Fukuoka, S. Yamanaka, and T. Takabatake, Appl. Phys. Lett. **92**, 041901 (2008).
[12] K. Suekuni, M. A. Avila, K. Umeo, and T. Takabatake, Phys. Rev. B **75**, 195210 (2007).
[13] K. Suekuni, Y. Takasu, T. Hasegawa, N. Ogita, M. Udagawa, M. A. Avila, and T. Takabatake, Phys. Rev. B **81**, 205207 (2010).
[14] F. Bridges and L. Downward, Phys. Rev. B **70**, 140201 (2004).
[15] Q. Xi, Z. Zhang, J. Chen, J. Zhou, T. Nakayama, and B. Li, Phys. Rev. B **96**, 064306 (2017).
[16] S. Christensen, M. S. Schmøkel, K. A. Borup, G. K. H. Madsen, G. J. McIntyre, S. C. Capelli, M. Christensen, and B. B. Iversen, J. Appl. Phys. **119**, 185102 (2016).
[17] R. E. Peierls, *Quantum Theory of Solids* (Oxford University Press, New York, 1955).
[18] L. Lindsay, Nanoscale Micro. Thermophys. Eng. **20**, 67 (2016).
[19] P. B. Allen and J. L. Feldman, Phys. Rev. B **48**, 12581 (1993).
[20] P.-F. Lory *et al.*, Nat. Commun. **8**, 491 (2017).
[21] D. J. Hooton, Philos. Mag. **3**, 49 (1958).
[22] T. R. Koehler, Phys. Rev. Lett. **17**, 89 (1966).
[23] P. Souvatzis, O. Eriksson, M. I. Katsnelson, and S. P. Rudin, Phys. Rev. Lett. **100**, 095901 (2008).
[24] I. Errea, M. Calandra, and F. Mauri, Phys. Rev. B **89**, 064302 (2014).

[25] T. Tadano and S. Tsuneyuki, Phys. Rev. B **92**, 054301 (2015).
[26] A. van Roekeghem, J. Carrete, and N. Mingo, Phys. Rev. B **94**, 020303 (2016).
[27] T. Tadano and S. Tsuneyuki, J. Phys. Soc. Jpn. **87**, 041015 (2018).
[28] G. Kresse and J. Furthmüller, Phys. Rev. B **54**, 11169 (1996).
[29] J. P. Perdew, K. Burke, and M. Ernzerhof, Phys. Rev. Lett. **77**, 3865 (1996).
[30] P. E. Blöchl, Phys. Rev. B **50**, 17953 (1994).
[31] G. Kresse and D. Joubert, Phys. Rev. B **59**, 1758 (1999).
[32] T. Tadano, ALAMODE, http://sourceforge.net/projects/alamode/.
[33] T. Tadano, Y. Gohda, and S. Tsuneyuki, J. Phys. Condens. Matter **26**, 225402 (2014).
[34] F. Zhou, W. Nielson, Y. Xia, and V. Ozoliņš, Phys. Rev. Lett. **113**, 185501 (2014).
[35] See Supplemental Material at http://link.aps.org/supplemental/10.1103/PhysRevLett.120.105901 for details of the computational conditions, anharmonic phonon dispersion relations, phonon lifetimes at various temperatures and cell volumes, and a comparison of the scattering phase space and the cubic coupling coefficients between the BTE and SCP + BTE methods, which includes Refs. [36–41].
[36] H. Monkhorst and J. Pack, Phys. Rev. B **13**, 5188 (1976).
[37] P. E. Blöchl, O. Jepsen, and O. K. Andersen, Phys. Rev. B **49**, 16223 (1994).
[38] K. Parlinski, Z. Q. Li, and Y. Kawazoe, Phys. Rev. Lett. **78**, 4063 (1997).
[39] R. Tibshirani, J. R. Stat. Soc. Ser. B Stat. Methodol. **58**, 267 (1996).
[40] T. Hastie, R. Tibshirani, and J. Friedman, *The Elements of Statistical Learning* (Springer, New York, 2009).
[41] T. Hastie, R. Tibshirani, and M. Wainwright, *Statistical Learning with Sparsity: The Lasso and Generalizations* (Chapman & Hall/CRC, Boca Raton, 2015).
[42] K. Momma and F. Izumi, J. Appl. Crystallogr. **44**, 1272 (2011).
[43] S.-I. Tamura, Phys. Rev. B **27**, 858 (1983).
[44] S. Pailhès, H. Euchner, V. M. Giordano, R. Debord, A. Assy, S. Gomès, A. Bosak, D. Machon, S. Paschen, and M. de Boissieu, Phys. Rev. Lett. **113**, 025506 (2014).
[45] W. Li, J. Carrete, G. K. H. Madsen, and N. Mingo, Phys. Rev. B **93**, 205203 (2016).
[46] V. J. Härkönen and A. J. Karttunen, Phys. Rev. B **94**, 054310 (2016).
[47] A. Auerbach and P. B. Allen, Phys. Rev. B **29**, 2884 (1984).
[48] T. Sun and P. B. Allen, Phys. Rev. B **82**, 224305 (2010).